

Identification technique for the Density-Gradient model

PETRU ANDREI

Department of Electrical and Computer Engineering
Florida State University and Florida A&M University
2525 Pottsdamer St., Tallahassee FL 32309
ROMANIA

Abstract: - A new identification technique is presented for the Density-Gradient model. This identification technique is based on two-dimensional Schrödinger computations and can be easily extended to three-dimensional computations. The model parameters are found by comparing the electron concentration computed by using the Density-Gradient model in nanoscale semiconductor structures to results obtained by using the effective-mass Schrödinger equation.

Key-Words: - Density-Gradient model, Schrödinger equation, quantum confinement.

1 Introduction

Parameter identification in phenomenological semiconductor models is one of the most important tasks in the modeling and analysis of a device. Before the model is used for the simulation of the semiconductor device, the model parameters should be carefully calibrated against more elaborate physical models. In the case of the Density-Gradient (DG) model, the electron and hole effective masses that enter in the equations of the DG model should be computed by using self-consistent Poisson-Schrödinger computations.

The existing methods for the computation of electron and hole effective masses are based on the comparison of the model with one-dimensional Poisson-Schrödinger computations. While this approach gives good results for devices in which the carriers are confined in only one direction, it is not appropriate for devices in which the carriers are confined in more than one direction. Such devices include short-channel MOSFETs and SOI transistors, FinFETs, etc.

In this article we calibrate the DG model against two-dimensional Schrödinger computations. We focus mainly on the computation of electron effective mass since it enters directly in the equations of the electron current density in n-channel transistors, which are widely used in integrated circuits. The article is structured as follows. In Section II we present the DG model at thermal equilibrium. The basic idea of our calibration approach is presented in Section III, which will be followed by Conclusions.

2 The Density-Gradient model

The Density-Gradient (DG) model has been extensively used in the literature for the analysis of quantum mechanical induced effects in semiconductor devices [1]. In the framework of the DG model, the electron and hole densities at thermal equilibrium can be computed by using the following partial differential equations:

$$\frac{2\nabla \cdot (b_n \nabla \sqrt{n})}{\sqrt{n}} + \varphi - \Phi_n(T) = 0 \quad (1)$$

and

$$\frac{2\nabla \cdot (b_p \nabla \sqrt{p})}{\sqrt{p}} - \varphi + \Phi_p(T) = 0, \quad (2)$$

where φ is the electric potential, n and p are the electron and hole concentrations in the semiconductor, and $\Phi_n(T)$ and $\Phi_p(T)$ are some functions that depend on the nature of electron and hole statistics used. For Boltzmann statistics:

$$\Phi_n(T) = \frac{kT}{q} \ln \frac{n}{n_i} \quad (3)$$

and

$$\Phi_p(T) = \frac{kT}{q} \ln \frac{n_i}{p}, \quad (4)$$

where T is the absolute temperature. For Fermi statistics $\Phi_n(T)$ and $\Phi_p(T)$ should be computed by solving numerically the following equations:

$$n = \frac{2N_c}{\sqrt{\pi}} F_{1/2} \left[\frac{q(\Phi_n + \varphi_{ref})}{kT} \right] \quad (5)$$

and

$$p = \frac{2N_v}{\sqrt{\pi}} F_{1/2} \left[\frac{q(-\Phi_p + \varphi_{ref}) - E_g}{kT} \right], \quad (6)$$

where N_c and N_v are the effective density of states in the conduction and valence bands, respectively, E_g is the gap energy and φ_{ref} is the reference potential with respect to which the electrostatic potential is measured. In equations (5)-(6) $F_\alpha(x)$ is the Fermi integral of order α and is defined as:

$$F_\alpha(x) = \int_0^\infty \frac{t^\alpha dt}{1 + \exp(t-x)}. \quad (7)$$

Quantum mechanical effects are “controlled” by parameters:

$$b_n = \frac{\hbar^2}{4r_n q m_n^*} \quad (8)$$

and

$$b_p = \frac{\hbar^2}{4r_p q m_p^*}, \quad (9)$$

where m_n^* and m_p^* denote the effective masses of the electrons and holes. r_n and r_p are dimensionless parameters that account for the statistics of electrons and holes in semiconductor devices. The values of r_n and r_p vary asymptotically from 1, when only the lowest energy subband is occupied (e.g. at low temperature), to 3 when other subbands become populated as well (e.g. at high temperature). It should be noted that quantum mechanical effects can be neglected by setting $b_n = b_p = 0$ in equations (1)-(2). In this case the electrostatic potential is given by $\varphi = \Phi_n(T) = \Phi_p(T)$. In order to model the carrier distribution in semiconductor devices, equations (1)-(2) should be subject to appropriate boundary conditions and must be solved self-consistently. More details about boundary conditions for equations (1)-(2) can be found in [2].

3 Calibration of the Density-Gradient model

In the case of the DG model, parameters r_n and r_p are unknown and should be regarded as empirical quantities that have to be determined by matching experimental data to microscopic calculations. The same observation is valid for the electron and hole effective masses. Due to the low-order approximations involved in the derivation of equations and (1)-(2), it is unrealistic to use the experimental values of m_n^* and m_p^* . Instead, these

two parameters should be treated as fitting parameters. Since m_n^* and r_n , as well as m_p^* and r_p appear in (8) and (9) as products, the identification method can be simplified by letting only one of these two parameters vary, while keeping the other one fixed. It is usually assumed that $r_n = r_p = 3$, so the calibration problem is reduced to the determination of the electron and hole effective masses.

It should be noted that there is no unanimous agreement on the values of m_n^* and m_p^* . In most of the existing methods, m_n^* and m_p^* are found by fitting the results obtained from the DG model to the results obtained by solving the Poisson and Schrödinger equations for long channel MOS devices. For example, by fitting the DG model to C-V curves computed through one-dimensional simulations in MOS diodes, Wettstein *et al* [3] found $m_n^* = 0.278m_0$, where m_0 is the free electron mass. This value is in reasonably good agreement with the value obtained by Connelly *et al* [4], $m_n^* = 0.258m_0$, but it is slightly larger than the value obtained by Asenov *et al* [5] $m_n^* = 0.175m_0$. The common feature of these identification methods is that they calibrate b_n and b_p against results obtained by solving the 1-D Schrödinger equation in the direction perpendicular to the oxide layer (the z -direction) of MOSFET devices. In this way, it is tacitly assumed that the motion of electrons and holes is quantized only in the direction perpendicular to the oxide and it is described by classical statistics in the other two directions. While this approach is appropriate for long devices, more accurate methods must be developed for situations where quantum effects are important in the other two directions. For example, in the case of short-channel MOSFET devices, the electric potential can vary significantly in the along-channel direction (the x -direction) and one expects that the electron motion in this direction is quantized as well. A more rigorous approach to the problem is to solve the two-dimensional Schrödinger equation in the xz plane and to calibrate the DG model against these results. An identification method for b_n that is based on this observation is presented below. Parameter b_n is found by fitting the results obtained with the DG model to the results obtained by solving the two-dimensional Schrödinger equation. In subsequent computations, the (100) surface orientation is assumed for silicon because it is typical for most fabricated MOS devices.

For (100) silicon, the total electron concentration is composed of electron concentrations in six elliptical subbands that correspond to two valleys with $m_{x,i}^* = m_{y,i}^* = m_t$, $m_{z,i}^* = m_l$ ($i=1,2$), two valleys with $m_{x,i}^* = m_{z,i}^* = m_t$, $m_{y,i}^* = m_l$ ($i=3, 4$), and two valleys with $m_{y,i}^* = m_{z,i}^* = m_t$, $m_{x,i}^* = m_l$ ($i=5, 6$). In the above formulas, $m_{x,i}^*$, $m_{y,i}^*$, and $m_{z,i}^*$ denote the principal effective masses of the constant-energy ellipsoid in subband i , associated with the motion parallel to the x , y , and z -direction, respectively, and $m_t = 0.19m_0$ and $m_l = 0.916m_0$ are the transverse and longitudinal effective masses of electrons. As previously argued, the electron motion is quantized in the x and z directions and it is described by classical statistics in the y -direction. In the effective mass approximation, the electron energy can be described by the time-independent Schrödinger equation:

$$\left[-\frac{\hbar^2}{2} \left(\frac{1}{m_{x,i}^*} \frac{\partial^2}{\partial x^2} + \frac{1}{m_{z,i}^*} \frac{\partial^2}{\partial z^2} \right) + \varphi_c(x, z) \right] \Psi_{i,j}(x, z) = E_{i,j} \Psi_{i,j}(x, z), \quad (10)$$

where $\varphi_c(x, z)$ is the confining potential in the xz plane measured with respect to the conduction band, while $\Psi_{j,i}(x, z)$ are the envelope wave functions associated with the j eigenvalue in subband i ($i=1, \dots, 6$), $E_{j,i}$. Once the eigenvalue problem (10) is solved, the electron concentration can be computed by summing over all energy states:

$$n(x, z) = \sum_{i=1}^6 \sum_j |\Psi_{i,j}(x, z)|^2 \int f_{i,j}(E) D_{i,j}(E) dE, \quad (11)$$

where $f_{i,j}(E)$ is the Fermi distribution function and

$$D_{i,j}(E) = \frac{1}{h} \sqrt{\frac{2m_{y,i}^*}{E - E_{i,j}}} \quad (12)$$

is the one-dimensional density of the states corresponding to electrons in subband i and energy level j . After performing the integration in (11), we obtain the following equation for the total electron concentration [6]:

$$n(x, z) = \sum_{i=1}^6 \frac{2\sqrt{2m_{z,i}^* kT}}{h} \sum_j F_{-1/2} \left(\frac{E_F - E_{i,j}}{kT} \right) |\Psi_{i,j}(x, z)|^2, \quad (13)$$

where E_F is the chemical potential that at room temperature is approximately equal to the Fermi

energy and $F_{-1/2}(x)$ is the Fermi integral of order $-1/2$.

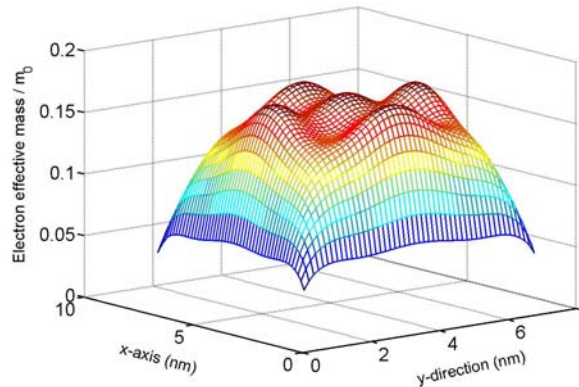


Fig. 1. Effective mass of electrons as computed from the Density-Gradient equation (1) and the Schrödinger equation (10) for Si(100).

In order to find parameter b_n , arbitrary (100) silicon systems were simulated by using the two-dimensional DG model and the two-dimensional Schrödinger equation. To avoid solving the Poisson equation many times, we assumed that the potential in equations (1) and (10) is given a priori and we compared the electron concentration distributions obtained by using these two equations. Parameter b_n was found by using the best fit between the two electron concentration functions.

3.1 Analytical solution for m_n^*

A special case in which the energy eigenstates can be found analytically is the two-dimensional rectangular quantum box with infinite walls. In this case, the electrostatic potential can be written as follows:

$$\varphi(x, z) = \begin{cases} V_0, & \text{if } 0 < x < L_x, \text{ and } 0 < z < L_z, \\ \infty, & \text{otherwise,} \end{cases} \quad (14)$$

while the energy eigenvalues and eigenfunctions are:

$$E_{i,j_x,j_z} = \frac{\hbar^2}{8} \left[\frac{j_x^2}{m_{x,i}^* L_x^2} + \frac{j_z^2}{m_{z,i}^* L_z^2} \right] \quad (15)$$

and

$$\Psi_{i,j_x,j_z}(x, z) = \frac{2}{\sqrt{L_x L_z}} \sin \left(\frac{j_x \pi x}{L_x} \right) \sin \left(\frac{j_z \pi z}{L_z} \right). \quad (16)$$

Electron concentration $n(x, z)$ can be computed by using equation (11).

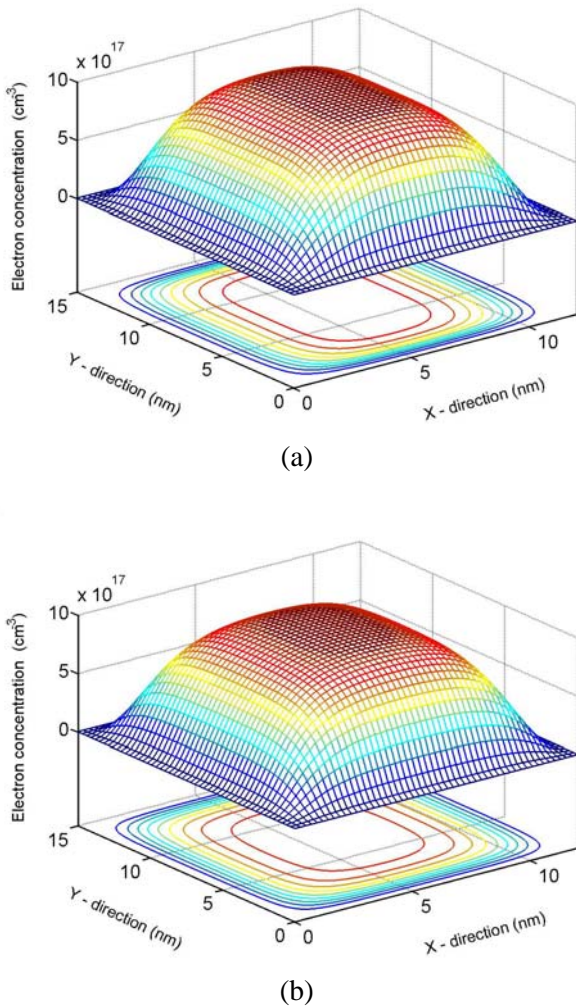


Fig. 2. Electron concentration computed by using the Density-Gradient model (a) and the Schrödinger equation (b) for a 10×15 nm rectangular box.

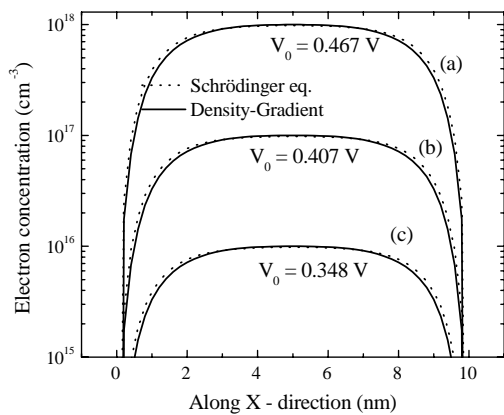


Fig. 3. Electron concentration cross-sections through the middle plane of a 10x15 nm rectangular quantum box.

It is remarkable that, in the case of a rectangular box, one can find analytical equations for the electron effective mass. If we assume that $b_n(x, z)$ varies relatively slowly with x and z [in fact the DG model predicts that b_n is constant—see equation (8)] and by using the first-order approximation one can find that:

$$b_n(x, z) \approx \frac{\sqrt{n}(\Phi_n(T) - \varphi)}{2\nabla^2 \sqrt{n}}. \quad (17)$$

In Figure 1 we have represented the electron effective mass computed by:

$$m_n^*(x, z) = \frac{\hbar^2}{4r_n q b_n(x, z)} \quad (18)$$

for a rectangular box with dimensions 6×10 nm. One can observe that m_n^* depends on the spatial coordinates. It can be approximated by $m_n^* = (0.17 \pm 0.01)m_0$, which is the value computed in the middle of the box.

In Figures 2(a) and 2(b) we have represented the electron concentrations in the quantum boxes computed by using $m_n^* = 0.17m_0$. In Figure 3 we use continuous lines to represent cross-sections through the middle plane ($x = 6$ nm) of the electron concentration, for different values of electric potential V_0 . The values of V_0 displayed in Figure 3 correspond to the Fermi levels in bulk silicon with doping concentrations of 10^{16} cm^{-3} , 10^{17} cm^{-3} , and 10^{18} cm^{-3} , respectively. The agreement between the electron concentrations obtained by using the two approaches is remarkably good and proves that the DG model can be successfully used for the modeling of electron and hole concentration in silicon.

It is instructive to note that, in general, the x and the z directions in the Schrödinger equation are not equivalent (e.g. in anisotropic systems) due to the different effective mass values in the expression of the Hamiltonian [see equation (10)]. These systems can be modeled in the framework of the DG model by using different values for the fitting parameters b_n and b_p along the two directions. This requires calibrating the electron and hole effective masses in both directions, which is a more complicated task. Fortunately, in the case of Si, the x , y , and z directions are equivalent because of the symmetry of the six valleys in the conduction band, and we can consider equal effective masses in these directions (denote them by m_n^*).

Figure 4 presents the computed values of m_n^* for different dimensions L_x and L_y of the quantum region. The continuous line shows the results obtained by keeping L_y at 15 nm (which is approximately the length of the

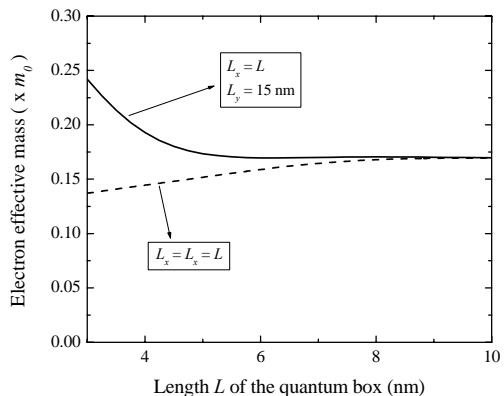


Fig. 4. Electron effective mass that gives the best agreement between the electron concentration computed by using the two-dimensional Schrödinger equation and two-dimensional DG model for a rectangular quantum box. The dimensions of the box are indicated on the abscissa.

conduction channel in ultra small MOSFET devices) and varying L_x from 3 nm to 10 nm. The dash line shows the values of the electron effective mass in the case when L_x and L_y are equal to each other and varied between 3 and 10 nm. We can observe that, for dimensions of the quantum box larger than 8 nm, the electron effective mass is almost constant and approximately equal to $0.17m_0$, which is in agreement with the simulations presented in Figure 1. For smaller dimensions of the quantum box, the value of m_n^* should be changed. For example, if one dimension of the quantum box decreases to 3 nm while the other one is larger than 8 nm, $m_n^* ; 0.24m_0$. In numerical simulations one should use the value of the electron effective mass which corresponds to the approximate size of the quantum region.

The electron concentrations obtained by using the DG model and the Schrödinger equations are represented in Figures 4(a) and 4(b) respectively. One can observe again that there is a very good agreement between the two methods.

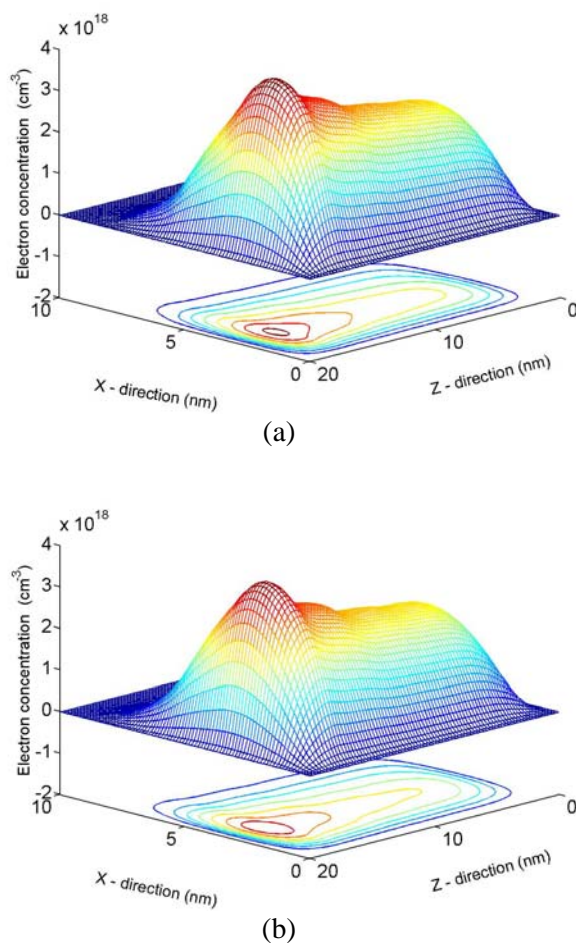


Fig. 5. Electron concentration computed by using the Density-Gradient model (a) and the Schrödinger equation (b) for a 10×15 nm rectangular box.

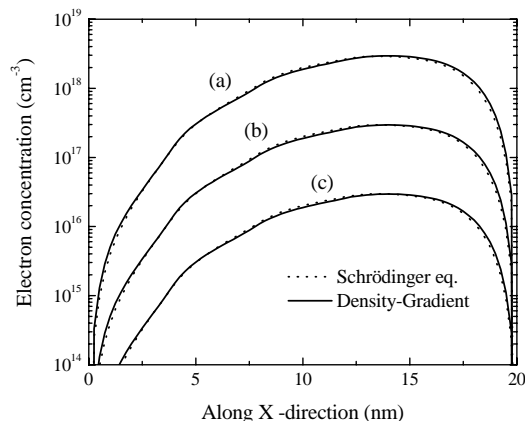


Fig. 6. Electron concentration cross-sections through the middle plane of a 10×20 nm rectangular quantum box.

3.2 Calibration of m_n^* for custom electric potentials

We also computed m_n^* for other potential functions and obtained very good agreement between the predictions of the DG model and of the two-dimensional Schrödinger equation. In these simulations, the Schrödinger equation was discretized by using the finite difference scheme and the eigenvalues and eigenfunctions of the energy were computed by using the LAPACK package [7]. In most cases, grids of 70×70 points were used, resulting in computation times of about three hours on a Pentium 4 (3 GHz) processor. These computation times should naturally be compared with the computation time required to find the electron concentration by using the DG model and which, in our simulations, is of the order of seconds on the same processor. Figure 5 (a) illustrates the electron concentration computed by using the Schrödinger equation with the following electric potential $\varphi(x, z) = V_0 + V_1 \exp\left(\frac{ax}{L_x}\right) - V_2 \exp\left(\frac{bz}{L_z}\right)$ if

$x < 10$ nm and $z < 20$ nm, and $\varphi(x, z) = \infty$, otherwise. In the last equation, V_0 , V_1 , V_2 , a , and b are given parameters. In these simulations we used: $V_0 = 348$ mV, $V_1 = 0.12$ mV, and $V_2 = 1.2$ mV, $a = 4$ nm, and $b = 2$ nm. The dimensions of the quantum region were 10×20 nm. This potential was chosen because it varies significantly in the box region and, in this way, it may reveal the ability of the DG model to describe electron concentrations for a broad class of potentials. The electron concentration computed by using the DG model is shown in Figure 5 (b).

In Figure 6 we use continuous lines to represent cross-sections through the middle plane ($x = 5$ nm) of the electron concentration, for the same values of the electric potential V_0 as in Figure 3. The good agreement between the Schrödinger and the DG calculations suggests once more that electron concentration can be accurately described by the DG model, provided that one performs proper calibration of the electron effective mass.

4 Conclusion

The parameters of the Density-Gradient model are carefully calibrated against Schrödinger computations. It is shown that the electron density can be reproduced accurately in two-dimensional quantum boxes with dimensions over 10 nm by

using the Density-Gradient model with the electron effective mass around $0.17m_0$. However, if the quantum box is smaller the electron effective mass might increase or decrease as a function of the shape and dimensions of the box. The values obtained for m_n^* are close to the transversal effective mass of electrons in silicon, which is in agreement with the fact that most contribution to the electron concentration in the conduction band is given by electrons with lower effective masses.

6 Acknowledgements

This work is supported by the Army High Performance Computing Research Center (AHPARC) under the auspices of the Department of the Army, Army Research Laboratory (ARL) under Cooperative Agreement number DAAD19-01-2-0014. The content does not necessarily reflect the position or the policy of the government and no official endorsement should be inferred.

References:

- [1] M. G. Ancona and G. J. Iafrate, "Quantum correction to the equations of state of an electron gas in a semiconductor," *Phys. Rev. B* **39**, 9536 (1989).
- [2] M. G. Ancona, Z. Yu, R. W. Dutton, P. J. V. Voorde, M. Cao, and D. Vook, "Density-Gradient analysis of MOS tunneling," *IEEE Trans. Electron Devices* **47**, 2310 (2000).
- [3] A. Wettstein, A. Schenk, and W. Fichtner, "Quantum device-simulation with the Density-Gradient model on unstructured grids," *IEEE Trans. Electron Devices* **48**, 279 (2001).
- [4] D. Connelly, Z. Yu, and D. Yergeau, "Macroscopic simulation of quantum mechanical effects in 2-D MOS devices via the Density Gradient method," *IEEE Trans. Electron Devices* **49**, 619 (2002).
- [5] A. Asenov, S. Slavcheva, A. R. Brown, J. H. Davies, and S. Saini, "Increase in the random dopant induced threshold fluctuations and lowering in Sub-100 nm MOSFETs due to quantum effects: a 3-D Density-Gradient simulation study," *IEEE Trans. Electron Devices* **48**, 722 (2001).
- [6] P. Andrei and I. Mayergoyz, "Analysis of fluctuations in semiconductor devices through self-consistent Poisson-Schrödinger computations," *J. Appl. Phys.* **96**, 2071 (2004).
- [7] <http://www.netlib.org/lapack>